CHEMISTRY
A EUROPEAN JOURNAL

DOI: 10.1002/chem.200500611

Controlled Self-Assembly of Amphiphilic Oligopeptides into Shape-Specific Nanoarchitectures

Tomoyuki Koga,[a] Masahiro Higuchi,[b] Takatoshi Kinoshita,[c] and Nobuyuki Higashi*[a]

Abstract: Here, we report a novel, programmable, molecular self-assembling system to fabricate shape-specific, three-dimensional nanoarchitectures. Three types of simple 16-mer peptides consisting of hydrophobic Leu and hydrophilic Lys, LKL16, KLK16, and LK16, were prepared as building blocks for nanofabrications. A detailed analysis of the conformation and self-assembling mechanism was performed by using circular dichroism (CD), FTIR spectroscopy, and atomic force microscopy (AFM). A wide variety of self-assembled nanoarchitectures, such as β-sheet-plates, β-sheet-fibers, α-helix-particles, and α-helix-plates, could be fabricated by tuning the peptide sequence, reaction time, and solution pH. The ability to control the self-assembled nanostructures should provide a simple and/or essential insight into the mechanism of peptide aggregation, including amyloid formation, and it should be useful for the design of novel bio-related nanomaterials.

Keywords: amphiphilic peptides · amyloids · conformation analysis · nanostructures · self-assembly

Introduction

The self-assembly of peptides, proteins, and their derivatives into shape-specific nanoarchitectures has attracted much attention as a powerful approach for designing novel functional nanomaterials, and because of their association with neurodegenerative diseases.[1–5] For example, the polymerization of the amyloid β-peptide (Aβ) into protease-resistant fibrillar deposits with an α-to-β structural change in the brain parenchyma and vasculature has been considered a significant step in the pathogenesis of Alzheimer's disease.[6] In previous studies, a total of at least 16 different proteins and peptides were identified in amyloid aggregates,[7,8] and these aggregates were found to have a common core structure (a straight, long, cross-β structure),[9] despite the fact that the proteins involved have no sequential or structural similarities. Nonpathogenic proteins and synthetic peptides also form nanofibers that structurally resemble in vivo fibrils.[10–14] Thus, the ability to form amyloid fibrils from a wide range of synthetic peptides gives access to a large number of model systems with which to study the process of fibril formation in more detail. However, despite extensive studies of amyloid fibrils that have resulted in the elucidation of many aspects of their underlying nature, important issues concerning their structure and mechanism of formation remain to be resolved. It is, therefore, important to construct peptide β-sheet assemblies and to elucidate their molecular structure, including their formation mechanism, to understand the pathogenesis of and therapeutics for the diseases with which they are associated.

On the other hand, from the standpoint of materials science, molecular self-assembly is a good candidate for a breakthrough technology that enables the fabrication of three-dimensional structures from the bottom-up on the scale between nanometers and submicrons. Peptides and proteins in particular are versatile building blocks for constructing nanomaterials; examples of their use as various scaffolds are found in nature. A number of artificial peptidemimetics have been prepared and reported to self-assemble into nanostructures, such as micelles,[15] vesicles,[16,17] fibers,[13,14,18] networks,[19,20] and a variety of other morpholo-

[a] Dr. T. Koga, Prof. N. Higashi
Department of Molecular Science & Technology
Faculty of Engineering, Doshisha University
Kyotanabe, Kyoto 610–0321 (Japan)
Fax: (+81) 774-65-6844
E-mail: nhigashi@mail.doshisha.ac.jp

[b] Prof. M. Higuchi
Department of Chemistry for Materials
Faculty of Engineering, Mie University
Tsu, Mie 514–8507 (Japan)

[c] Prof. T. Kinoshita
Department of Life & Materials Engineering
Nagoya Institute of Technology
Gokiso-cho, Showa-ku, Nagoya 466–8555 (Japan)

Supporting information for this article is available on the WWW under http://www.chemeurj.org/ or from the author.

gies.[21] These self-organized protein architectures are expected to have potential as novel biomaterials with a wide range of applications, such as bioscaffolds, nanoreactors, nanocarriers, and nanotemplates, depending on their three-dimensional nanostructures. If the self-assembling behavior of peptides on the nanoscale can be controlled precisely by tuning the molecular structure and/or environment, that is, self-assembly can be programmed, nanofabrications of designed and more complicated three-dimensional objects could be accomplished more easily, quickly, and accurately than by the conventional top-down approaches.

Here, we report the controlled self-assembly of amphiphilic oligopeptides into shape-specific nanoarchitectures. Three types of simple 16-mer peptides consisting of hydrophobic Leu and hydrophilic Lys were prepared and used as building blocks for nanofabrication. A detailed analysis of the conformation and self-assembling mechanism was performed, with consideration of both molecular structure and environmental factors. These studies should provide useful information, not only for understanding the mechanism of peptide aggregation, including amyloid formation, but also for developing novel peptide-based nanomaterials.

Results and Discussion

To obtain simple and/or essential information about the peptide aggregation involved in amyloid formation, and to fabricate the designed nanoarchitecture, we used three types of simple amphiphilic peptides composed of Leu and Lys as building blocks for molecular self-assembly. For in vivo systems, it has been assumed that hydrophobic defects, derived from hydrophobic amino acid sequences, induce molecular aggregation for many amyloidogenic peptides. For example, the Aβ(1–40/42) peptides contain two hydrophobic domains, comprising residues 17–21 and residues 29–40/42. The LKL16, LK16, and KLK16 were also designed to have a tetra-Leu domain, which provided the hydrophobic driving force for self-assembly, and was located at either both ends (N and C termini), at one end (C terminus), or in the center of the peptide, respectively (Figure 1). These peptides should clarify the effect of the arrangement of the hydrophobic Leu domain in the peptide chain on their self-assembling properties in water. In addition, we anticipated that it might be possible to control the distribution of the high-order structures by manipulating conditions, such as pH and ionic strength, owing to perturbations of peptide chains, dependent on the charged condition of the Lys residues.

The conformational properties of the peptides were first investigated by circular dichroism (CD) and FTIR spectroscopic analysis. Figure 2 show the CD spectra for KLK16, LK16, and LKL16, respectively, at various pHs ([peptides] = 40 μM), just after preparation of sample solutions. For KLK16 and LK16, the spectra show a pattern typical of right-handed helical peptides with two negative maxima, one at 222 nm and one at 204 nm, in the high pH region of 10.6 (Figure 2a and b). By lowering the pH value to 5.8, the

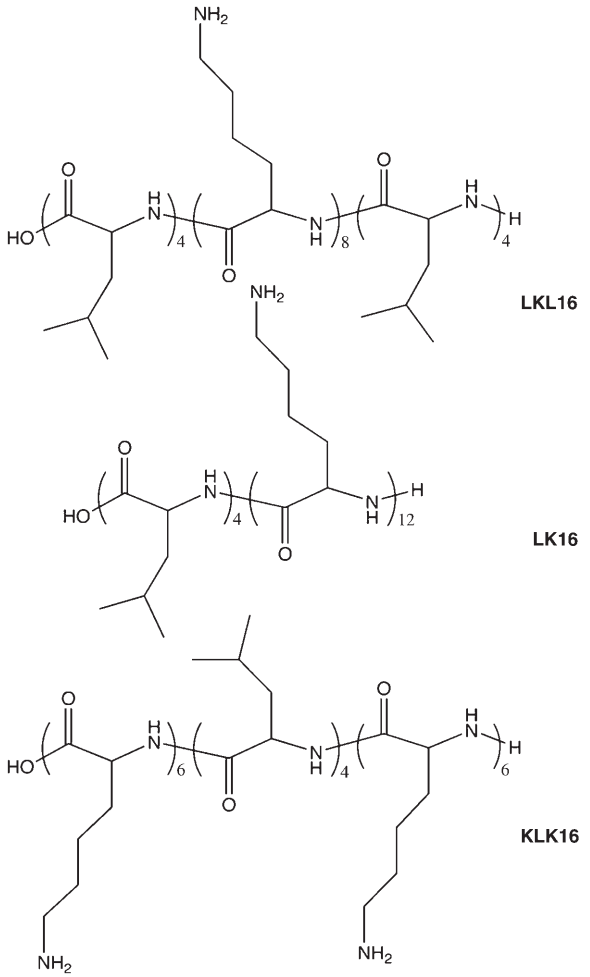

Figure 1. Molecular structures of the amphiphilic 16-mer peptides, LKL16, LK16, and KLK16, which were used as building blocks for nanofabrication.

spectra change to that of random coil structures (negative peak at 198 nm) through an isodichroic point at around 202 nm. These CD spectra were time-independent within the period of one week. On the other hand, the conformational properties of LKL16 differ considerably from those of LK16 and KLK16, as shown in Figure 2c. Although the LKL16 also existed as a random coil structure at pH 5.8, the structural transition into a β-sheet (single negative maximum at 217 nm) was observed by increasing the pH value up to 9.4. Above pH 9.5, the CD spectra showed the aggregated β-sheet structure, as evidenced by the red-shifting of the 217 nm band toward 220 nm, reduction in ellipticity, and deviation from the isodichroic point. This result was also supported by atomic force microscopy (AFM, described later). Interestingly, in the case of LKL16, the spontaneous conformational transition with incubation time was observed within the narrow pH range of 8.8–9.4. Figure 3 shows the time dependence of CD spectra for LKL16 at pH 9.2. With freshly prepared sample solution, the spectrum initially showed a mixed pattern of α-helix and random coil structures, and then revealed a gradual change typical for a β-

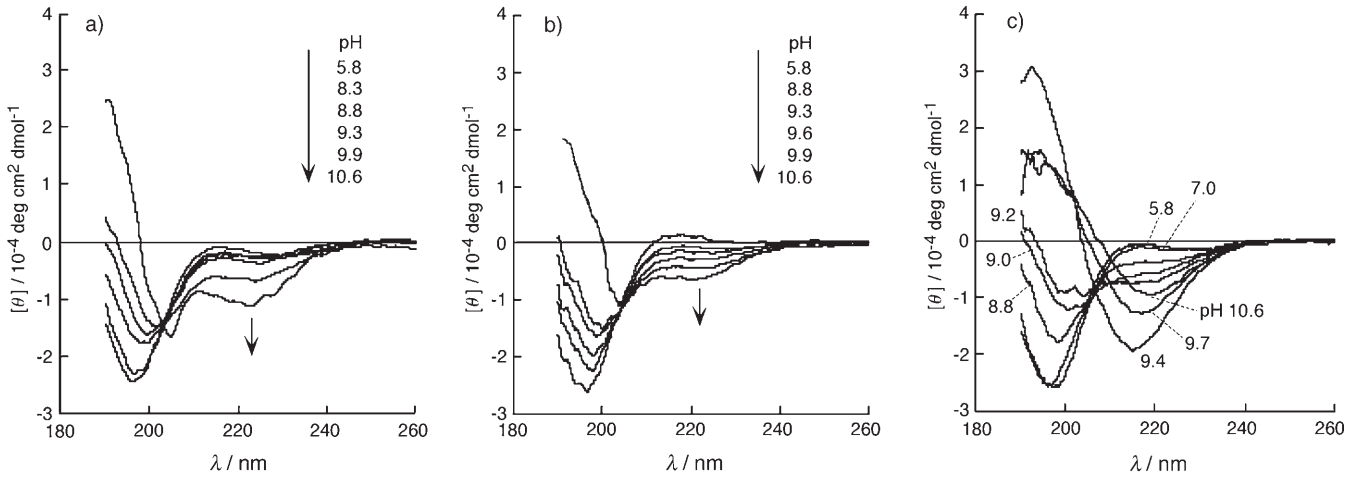

Figure 2. Conformational analyses of the peptides in aqueous media (containing 5% TFE) under various conditions. CD spectra of KLK16 (a), LK16 (b), and LKL16 (c), at the various pHs indicated (5.8–10.6). [peptides] = 40 μM.

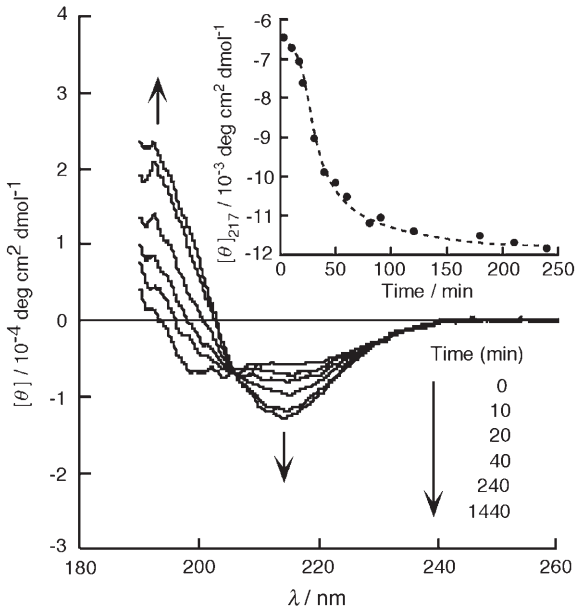

Figure 3. CD spectral change of LKL16 at pH 9.2. The peptide was incubated at RT for the time indicated (0–1440 min). The inset shows the time dependence of the molar ellipticity at 217 nm ($[\theta]_{217}$) under these conditions. [LKL16] = 40 μM.

sheet through an isodichroic point at 205 nm after 24 h. Transmission FTIR spectra provided more detailed information regarding the secondary structure. In the amide I region,[22] characteristic absorptions of an antiparallel β-sheet structure were observed at 1687 and 1625 cm^{-1} for LKL16 after incubation for 24 h at pH 9.2 (see Figure S1, Supporting Information), whereas such β-sheet formation was not observed for KLK16 and LK16 (peak maxima at 1670 cm^{-1} in both cases). Figure 3 inset shows the plot of molar ellipticity at 217 nm ($[\theta]_{217}$) as a function of time. As time lapsed, the $[\theta]_{217}$ value decreased sigmoidally, and reached a constant value after about 200 min. A nucleation-dependent polymerization model has been proposed to explain the mechanisms of amyloid formation by a variety of disease-related proteins,[23–25] and it has been well established as the fundamental mechanism of crystal growth.[26] In this model, nucleus formation requires a thermodynamically unfavorable step involving association with protein monomer, and as a result, a lag phase was observed before aggregation and/or conformational transition of proteins and peptides. In our case, conformational transition of LKL16 was also accelerated at around 10–50 min, suggesting the similarity in transition kinetics between LKL16 and authentic amyloids. In addition, such spontaneous β-sheet formation was found to be concentration dependent. The critical aggregation concentration (cac) of the LKL16 was determined by using pyrene as a fluorescent probe at pH 9.2. Solutions of LKL16 at concentrations ranging from 10^{-8} to 10^{-4} M were prepared with a constant pyrene concentration (6.1×10^{-7} M), and the excitation spectra were recorded. A red-shift of the pyrene band from 335 to 339 nm was observed upon increasing the peptide concentration (Figure 4a). This change reflects the transfer of pyrene from water into the hydrophobic part of the peptide aggregate. A plot of the ratio of the intensity of the signal at 339 nm to that at 335 nm (I_{339}/I_{335}) versus the LKL16 concentration (Figure 4b) resulted in a cac value of around 5 μM. At concentrations below cac, the LKL16 did not form a β-sheet structure, even after incubation. Notably, aggregate formations by KLK16 and LK16, which form α-helix structures instead of β-sheet structures, were also suggested from the results of fluorescence studies at pH 10.6. The cac values of KLK16 and LK16 were evaluated to be 12 and 25 μM, respectively, which are somewhat higher than the value for LKL16, probably due to the differences in total hydrophobicity and/or conformation of the peptides.

These designed peptides showed the diverse self-assembly that depends on the variety of conformational properties. AFM is a useful technique for evaluating three-dimensional structural features of proteins and their assemblies on the nanometer scale, and provides significant information on the

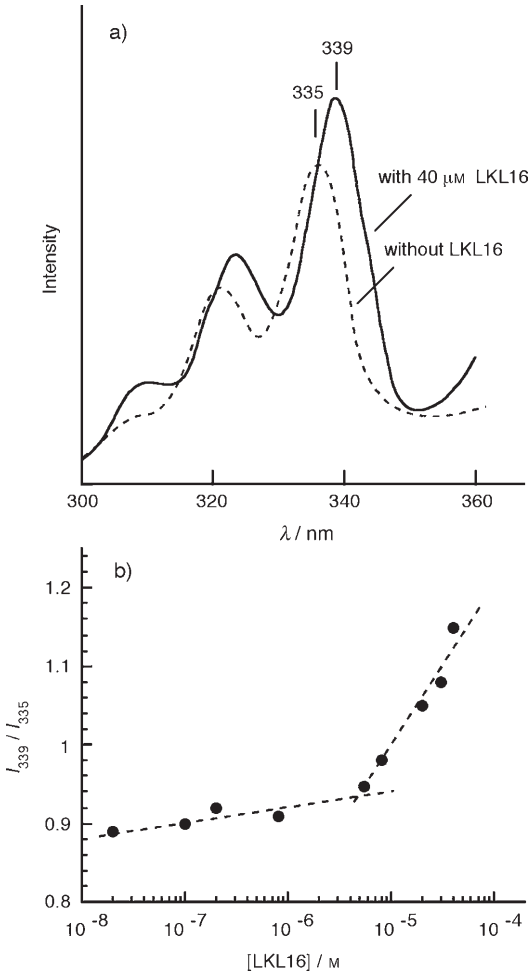

Figure 4. a) Fluorescence excitation spectra of pyrene (0.61 μM) with and without LKL16 (40 μM) at pH 9.2. b) Intensity ratio I_{339}/I_{335} at pH 9.2 obtained from the fluorescence excitation spectra of pyrene plotted against LKL16 concentration.

process of peptide aggregation. It is, however, well known that the convolution of the scanning tip leads to an overestimation of the sample's width.[27] All sample dimensions were, therefore, estimated mainly from the measured height of the sample shown in cross-section. Figure 5 shows the hierarchical self-assembly of LKL16 associated with the β-sheet formation at pH 9.2. A tapping-mode (TM)-AFM image obtained after 3 min revealed the presence of only globular aggregates (Figure 5a). The average height of the globular species was determined to be 0.8 ± 0.3 nm, indicating that the LKL16 exists in aqueous solution as a monomer. After incubation for 30 min, tape-like aggregates with a height of 1.6 ± 0.3 nm (average width 11 nm at AFM level) were newly observed, together with the globular species (Figure 5b). Herpar et al. reported that the Aβ protofibril elongation involved both the incorporation of monomers and the association of immature protofibrils.[28] In our case, it seems that the tape-like aggregates are also formed by the association of monomeric globular species. In addition, the actual width of the tape-aggregates can be calibrated from the observed width ($W_{obs}=11$ nm) to be 5.7 nm by using the following equation;[29] $W=W_{obs}-2(R_tH-H^2)^{1/2}$, in which the aggregate is assumed to be a plate, H is the observed height, and R_t is the radius of the AFM tip. This calculated value is consistent with the expected molecular length of a 16-residue peptide in β-sheet conformation (5.4 nm). It can be considered, therefore, that pairs of β-sheets build up the tape-like aggregate in a face-to-face manner, presumably by interacting through the Leu residues (see Figure 8). Amyloid-like peptide nanofibers with a different nanostructure were observed instead of globular species after incubation for 5–24 h (Figure 5c–f). Two types of fibers with lengths in excess of 1 μm and with different diametric ranges can be clearly distinguished in this image (Figure 5c). The type I fiber possesses a diameter of around 6.0 nm and a clearly visible left-handed twist that repeats along the fiber length (Figure 5d, amplitude image). The periodicity of this repeat is 45 ± 5 nm, and the fiber height varies between 5.5 nm and 6.5 nm. Although we have no direct evidence for the process of fiber formation, the molecular dimensions of the observed tape and type I fiber suggest that the three or four tapes form the type I fiber by associating with each other and then twisting along the fiber axis.[30] The observed left-handed twists of type I fibers are probably due to the chirality of the amino acids (L-isomers) in the constituent peptide species. However, the type II fiber was found to construct itself by intertwisting of the two type I-fibers. Figure 5e clearly reveals the branched and intertwisted structure of such type II fibers. From these height profiles, the maximum diameter of the type II fiber (ca. 12 nm) was consistent with the sum of the two type I fibers, each of diameter 6.0 nm, and the periodicity along the fiber length was 65 ± 5 nm (the difference between the maximum and minimum heights along the axis was ca. 4.5 nm). Furthermore, the observed fiber morphology of the branched structure on both sides of the type II fiber provides a plausible mechanism for the type I-to-type II fiber transition observed under the present conditions; two type I fibers contact and/or superpose upon each other at a point on the type I fiber, then they twist from this contact point (see Figure 8). Two such wound amyloid fibrils similar to the type II fiber were also observed in Alzheimer's disease (AD) brain tissue sections in in vivo studies.[31,32] An amyloid-like ordered structure of the LKL16 fiber was also supported strongly by results of a Congo red (CR) binding study. CR is a sulfonated azo dye that binds preferentially, but not exclusively, to protein and peptide species that adopt a cross-β amyloid structure.[33] Figure 6 shows an optical microscope image obtained under cross-polarized light and reveals the LKL16 fibers stained with CR. The stained peptide fibers exhibited a birefringence under cross-polarized light, demonstrating their anisotropy, and, therefore, indicating the presence of a regular quaternary structure, as was observed in authentic amyloids.

The morphological property of LKL16 was strongly affected by solution pH, which could induce the perturbation of secondary structure in response to the charged condition of amino groups on the Lys residues (see Figure S2, Sup-

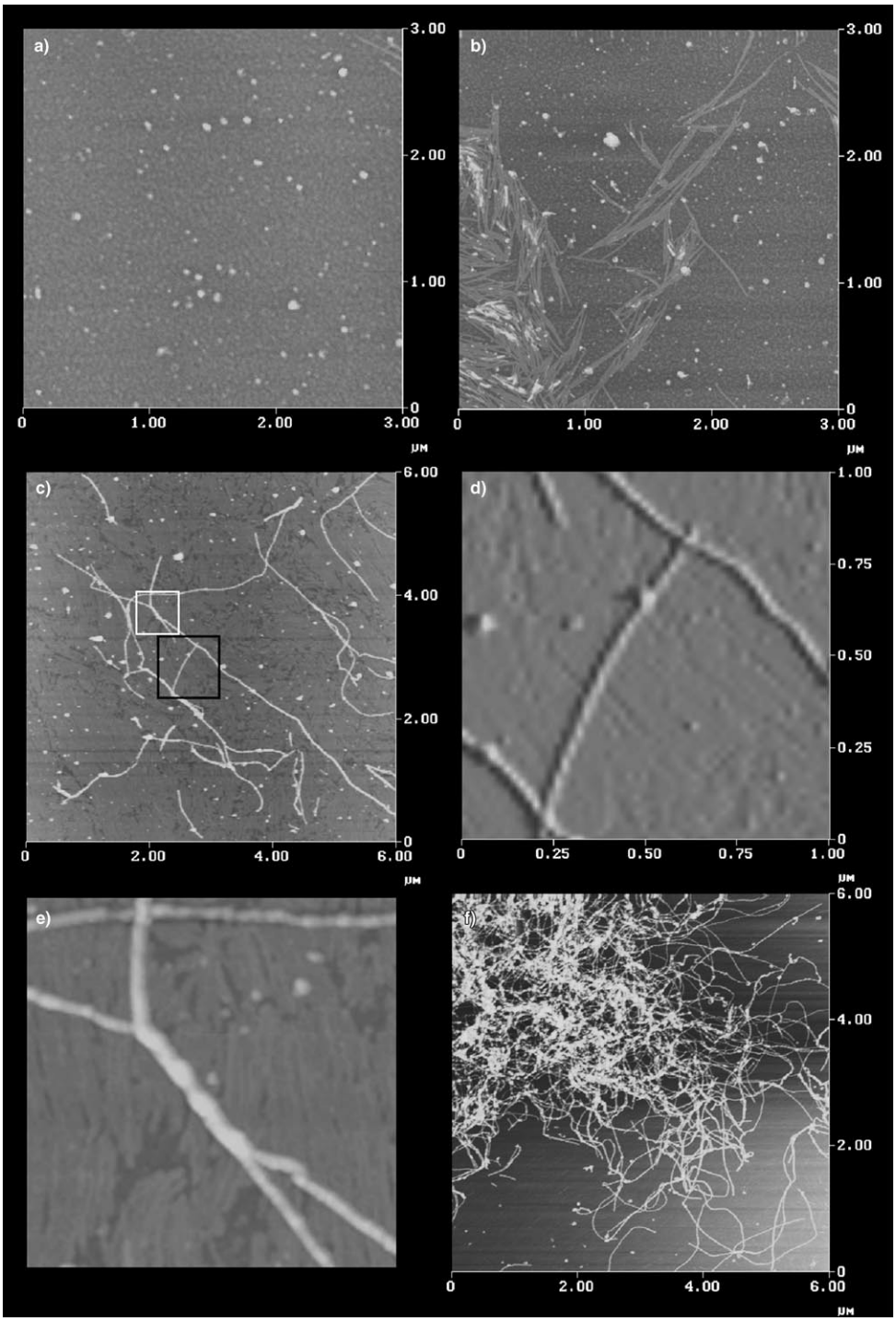

Figure 5. Hierarchical self-assembly of LKL16 (40 μM) into nanofibers at pH 9.2 and RT. Tapping-mode AFM images (3×3 μm^2 (a and b), 6×6 μm^2 (c and f)) obtained after incubation for 3 min (a), 30 min (b), 8 h (c), and 24 h (f). z-scale; 35 nm. d) Amplitude AFM image of a type I fiber, corresponding to the area marked with a black square in image (c). The average diameter is around 6.0 nm, and the twist repeat along the fiber axis is left-handed, with a periodicity of around 45 nm. e) Magnitude AFM image of a type II fiber, corresponding to the area marked with a white square in image (c). The type II fiber (diameter ca. 12 nm) was constructed by the intertwisting of the two type I fibers.

porting Information). In the lower pH region (7.0), at which LKL16 had positively charged amino groups, no aggregation was observed, indicating that LKL16 is predominantly in the monomeric random coil conformation (Figure S2a). On the other hand, at a higher pH of 10.6, the peptide was assembled rapidly with a β-sheet conformation (suggested by CD results), and formed poorly organized amorphous aggregates (Figure S2c). At pH 10.6, the positive charges present on the LKL16 will be shielded or will disappear. This increased tendency for intermolecular interactions between peptides, which causes the rapid aggregation of LKL16, is due to a drastic decrease in electrostatic repulsion and an increase in hydrophobicity. Such rapid aggregation of LKL16 seems to restrict mobility of the peptide chains, which prevents appropriate packing of peptide chains necessary for further organization. Thus, it seems that the development of regular intermolecular interactions involving extended regions of peptides is important for the formation of a highly organized nanofiber. At pH 9.2, the amino groups of LKL16 are partly protonated, and this charge will probably provide sufficient intermolecular repulsion to permit the controlled growth of fibers, as well as sufficient mobility of peptide chains for appropriate packing.

Self-fabricated nanostructures from peptide building blocks could also be controlled by tuning the peptide sequence, namely the arrangement of the hydrophobic Leu domain in the peptide chain. Figure 7 shows the TM-AFM images of α-helical LK16 and KLK16 after incubation for 24 h at pH 10.6. Prolonged incubation (one week) caused no significant morphological or conformational changes in either LK16 or KLK16. From Figure 7a, it is apparent that spherical aggregates with heights of around 3.0–5.0 nm were formed from LK16. The measured dimensions of these aggregates are in good agreement with twice the molecular length of LK16

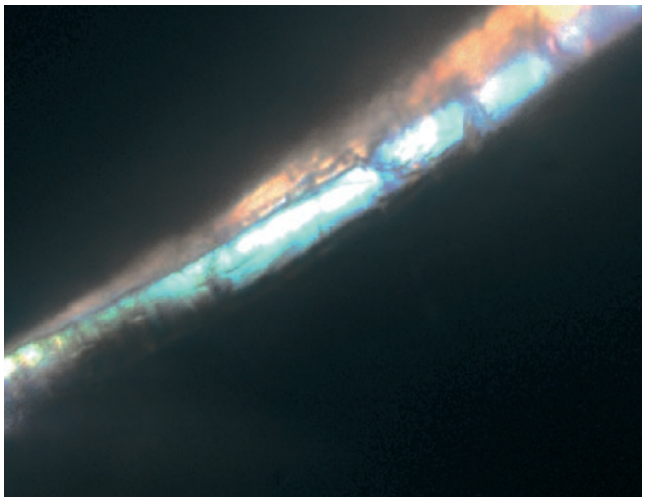

Figure 6. Optical microscope image obtained under cross-polarized light and showing the LKL16 fiber stained with Congo red. The fibrillar LKL16 assembly was obtained after incubation for 24 h at pH 9.2.

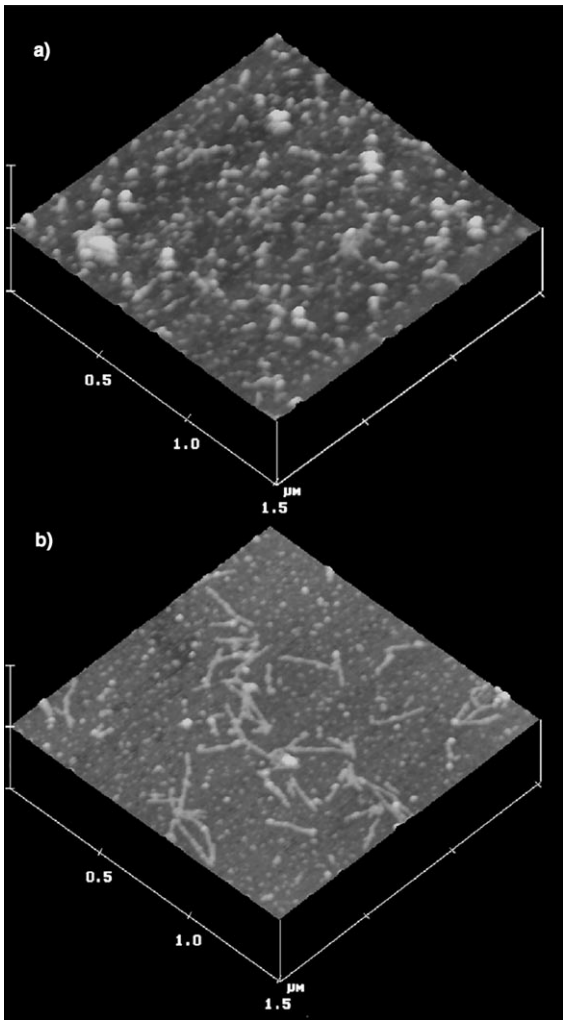

Figure 7. Three-dimensional TM-AFM images ($1.5 \times 1.5\ \mu m^2$) of LK16 (a) and KLK16 (b) after incubation for 24 h at pH 10.6 and RT. [peptides] = 40 μM. z-scale; 60 nm.

(ca. 2.4 nm), calculated by considering the conformation of the complete helix; the length of helix with $n = 16$ can be computed by using the occupied length (0.15 nm) of one amino acid residue along the helix axis. This result indicates the formation of a micelle-like structure consisting of a hydrophobic Leu domain core and the shell of a Lys domain (see Figure 8). The LK16 has the tetra-Leu domain at only one chain terminus, and this diblock-type structure will probably stabilize such micelle-structures. On the other hand, the α-helical KLK16, in which the tetra-Leu domain was arranged at the center, self-assembled into plate-shaped aggregates with heights of around 1.5 nm and lengths of 100–500 nm (Figure 7b). The observed heights of the plates correspond to the diameter of a polylysine helix (ca. 1.4 nm). Therefore, these plate-shaped aggregates probably consist of helix monolayers, in which KLK16 helices interact with each other in two dimensions, through the hydrophobic interaction between Leu residues located at the center (see Figure 8). Moreover, the helix–macrodipole interaction (namely, the head-to-tail antiparallel orientation of the KLK helices, which is energetically more favorable) may also contribute to the stability of the plate-shaped, high-order structure. The dipole moments of amino acids in an α-helical peptide align in the same orientation, nearly parallel to the helix axis. The resulting macroscopic dipole then generates an electrostatic potential, directed from the N terminus to the C terminus.[34] We reported direct evidence for a helix–helix macrodipole interaction obtained by exploring an attractive interaction between the disulfide-modified poly(L-glutamic acid) PLGA self-assembled monolayer on gold and redox-active PLGA derivatives as guest helices.[35] Thus, this electrostatic field, as well as the hydrophobic interaction and hydrogen bonding, should be one of the useful mediators for the assembly of high-order structures of protein/peptide architectures.

Conclusion

We have demonstrated a powerful strategy for fabricating novel supramolecular nanoarchitectures by the controlled self-assembly of peptide building blocks, as summarized in Figure 8. By tuning the peptide sequence and environmental conditions, such as solution pH and reaction time (input information), a wide variety of self-organized, three-dimensional architectures with various nanostructures were obtained (output information) by these self-assembling systems. In addition, the purely synthetic simple peptide LKL16 formed an amyloid-like nanofiber with structural transition under appropriate conditions, as did the other proteins associated with neurodegenerative diseases. These studies should make an important contribution, not only to our understanding of the mechanisms of protein aggregation, but also in establishing a novel and programmable molecular self-assembling system for the fabrication of designed three-dimensional nanoarchitectures.

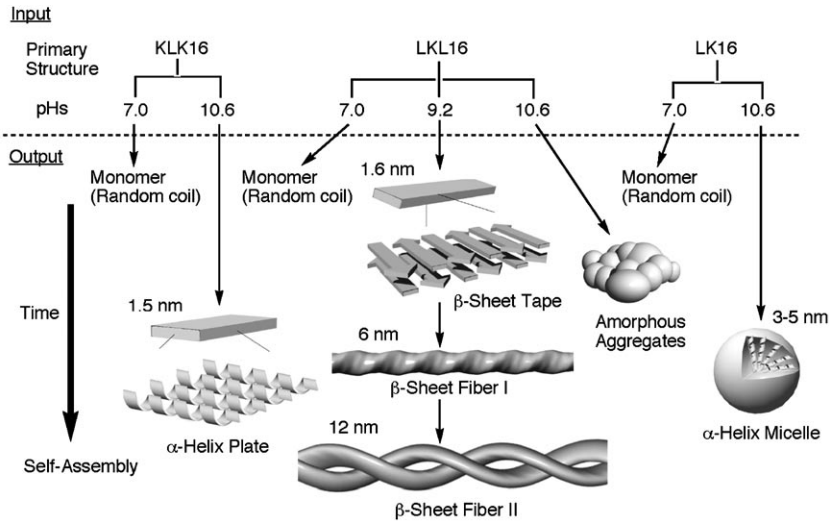

Figure 8. Schematic illustration summarizing the nanofabrication of three-dimensional architectures by the controlled self-assembly of the amphiphilic oligopeptides. By controlling the peptide sequence and environmental factors, such as pH and reaction time (input information), a wide variety of three-dimensional peptide architectures with various nanostructures could be spontaneously constructed (output information) by this molecular system.

Experimental Section

Peptide preparation: The amphiphilic 16-mer oligopeptides (LKL16, KLK16, and LK16) used in this study were prepared by solid-phase peptide synthesis using 9-fluorenylmethoxycarbonyl (Fmoc) chemistry. The peptide chains were synthesized on a CREAR (cross-linked ethoxylate acrylate resin, Peptide Institute), by using Fmoc-amino acid derivatives (3 equiv), 1-hydroxy-7-azabenzotriazole (3 equiv), and 1,3-diisopropylcarbodiimide (3 equiv) in *N,N*-dimethylformamide (DMF) for coupling, and piperidine (25%)/DMF for Fmoc removal. To cleave the peptide from the resin and to remove the side-chain-protecting groups, the peptide resins were treated with trifluoroacetic acid (TFA)/CH_2Cl_2 (9:1 *v/v*). The crude peptides were purified by performing reversed-phase HPLC (Bio-Rad, DuoFlow) with a YMC-Pack Pro C18 column (20×150 mm) by using a linear gradient of water/acetonitrile (containing 0.1% TFA). The purified peptides were identified by conducting MALDI-TOF MS (Shimazu KOMPACT MALDI III) and ^{1}H NMR spectroscopy (400 MHz, JEOL FX-400). All peptides were dissolved in 2,2,2-trifluoroethanol (TFE) as a stock solution before the aggregation assay. The aggregation solutions of the peptides (final peptide concentration: 40 μM, TFE content: 5%) were prepared by diluting the stock solution with 5 mM Tris/HCl buffer and aqueous NaOH. All the incubations for the aggregation of the peptides were performed at room temperature.

MALDI-TOF MS (see Figure S3, Supporting Information): *m/z* calcd for LKL16 $[M+H]^+$: 1949.9; found: 1948.4; *m/z* calcd for KLK16 $[M+H]^+$: 2007.4; found: 2007.6; *m/z* calcd for LK16 $[M+H]^+$: 2007.4; found: 2006.6. ^{1}H NMR analyses also gave satisfactory results (see Figure S4, Supporting Information).

Circular dichroism (CD) and FTIR spectroscopy: CD spectra were recorded by using a J-720 spectropolarimeter (JASCO) under a nitrogen atmosphere. Experiments were performed by using a quartz cell with a 5 mm path length over the range of 190–260 nm at ambient temperature. Sample solutions were prepared by diluting the TFE stock solution of peptides with buffer. Final peptide concentration was 40 μM in aqueous media. Transmission-FTIR spectra were measured by using CaF_2 plates with the Perkin–Elmer Spectrum 2000, and a mercury–cadmium–tellurium (MCT) detector (resolution, 2 cm^{-1}; number of scans, 1024). The peptides (LKL16, KLK16, and LK16) were adsorbed onto CaF_2 plates after incubation for 24 h at pH 9.2. The sample and the detector chambers were purged with dried nitrogen before and during measurement.

Atomic force microscopy (AFM): The AFM images were collected at ambient temperature by using a Nanoscope IIIa (Digital Instruments), which was operated by tapping with a supersharp silicon tip (tip radius 3 nm). An aliquot (10 μL) of the sample (LKL16, LK16, or KLK16) in buffer (containing 5% TFE) was placed on freshly cleaved mica. After adsorption for 2–30 min under moist conditions, the excess solution was removed by absorption onto filter paper. The resultant substrates were rinsed with buffer (30 μL, twice) to remove salt and the loosely bound peptide, and the samples were stored in a covered container to protect them from contamination until they were imaged (within 1–2 h). A 10 μm×10 μm scanner was used for imaging. The scanning speed was at a line frequency of 1 Hz, and the original images were sampled at a resolution of 512×512 points.

Fluorescence spectroscopy: Fluorescence studies were conducted by using a FP770 spectrofluorometer (JASCO). Experiments were performed at room temperature by using a quartz cell with a 10 mm path length. By using pyrene (Wako Pure Chemical Industries) as the probe molecules, a stock solution in buffer was prepared. Peptide samples were dissolved in the TFE stock solution, then diluted to specific concentrations with pyrene-containing buffer. Final pyrene concentration was 6.1×10^{-7} M. Excitation was performed from 300 to 360 nm, with 390 nm as the emission wavelength, 5 h after preparation of the sample solutions.

Congo red binding study: A Congo red (CR) (Wako Pure Chemical Industries) stock solution (150 μM) was prepared by dissolving the dye in buffer (pH 9.2) containing NaCl. CR binding studies were performed by diluting the incubated sample solutions (LKL16, 24 h incubation in 5 mM Tris/HCl buffer at pH 9.2) with the CR solution. The final concentration of CR was 5 μM in buffer at pH 9.2, and this included 100 mM NaCl. The resulting solution was incubated at room temperature for 3 h, then 50 μL was placed on a microscope slide and dried. The slide was examined under a microscope (Olympus Optical, BX50–34-FLAD-1) by using a cross-polarized light (magnification ×1000).

Acknowledgement

This work was supported in part by a grant-in-aid for scientific research from the Ministry of Education, Culture, Sports, Science and Technology of the Japanese Government.

[1] S. B. Prusiner, *Science* **1991**, *252*, 1515–1522.
[2] J. D. Sipe, *Crit. Rev. Clin. Lab. Sci.* **1994**, *31*, 325–354.
[3] P. T. Lansbury, *Proc. Natl. Acad. Sci. USA* **1999**, *96*, 3342–3344.
[4] C. M. Dobson, *Trends Biochem. Sci.* **1999**, *24*, 329–332.
[5] L. C. Serpell, *Biochim. Biophys. Acta* **2000**, *1502*, 16–30.
[6] D. J. Selkoe, *J. Biol. Chem.* **1996**, *271*, 18295–18298.
[7] J. W. Kelly, *Curr. Biol.* **1998**, *8*, 101–106.
[8] J. C. Rochet, P. T. Lansbury, *Curr. Biol.* **2000**, *10*, 60–68.
[9] M. Sunde, C. C. F. Blake, *Adv. Protein Chem.* **1997**, *50*, 123–159.
[10] F. Chiti, P. Webster, N. Taddei, A. Clark, M. Stefani, G. Ramponi, C. M. Dobson, *Proc. Natl. Acad. Sci. USA* **1999**, *96*, 3590–3594.

[11] M. Fandrich, M. A. Fletcher, C. M. Dobson, *Nature* **2001**, *410*, 165–166.
[12] Y. Fezoui, D. M. Hartley, D. M. Walsh, D. J. Selkoe, J. J. Osterhout, D. B. Teplow, *Nat. Struct. Biol.* **2000**, *7*, 1095–1099.
[13] Y. Takahashi, A. Ueno, H. Mihara, *Chem. Eur. J.* **1998**, *4*, 2475–2484.
[14] H. A. Lashuel, S. R. LaBrenz, L. Woo, L. C. Serpell, J. W. Kelly, *J. Am. Chem. Soc.* **2000**, *122*, 5262–5277.
[15] G. W. Vandermeulen, C. Tziatzios, H. A. Klok, *Macromolecules* **2003**, *36*, 4107–4114.
[16] S. Vauthey, S. Santoso, H. Gong, N. Watson, S. Zhang, *Proc. Natl. Acad. Sci. USA* **2002**, *99*, 5355–5360.
[17] J. R. Hernandez, S. Lecommandoux, *J. Am. Chem. Soc.* **2005**, *127*, 2026–2027.
[18] T. Koga, K. Taguchi, Y. Kobuke, T. Kinoshita, M. Higuchi, *Chem. Eur. J.* **2003**, *9*, 1146–1156.
[19] W. A. Petka, J. L. Harden, K. P. McGrath, D. Wirtz, D. A. Tirrell, *Science* **1998**, *281*, 389–392.
[20] A. P. Nowak, V. Breedveld, L. Pakstis, B. Ozbas, D. J. Pine, D. Pochan, T. J. Deming, *Nature* **2002**, *417*, 424–428.
[21] J. D. Hartgerink, E. Beniash, S. I. Stupp, *Science* **2001**, *294*, 1684–1688.
[22] T. Miyazawa, E. R. Blout, *J. Am. Chem. Soc.* **1961**, *83*, 712–719.
[23] J. T. Jarrett, P. T. Lansbury, *Biochemistry* **1992**, *31*, 12345–12354.
[24] A. Lomakin, D. S. Chung, G. B. Benedek, D. A. Kirschner, D. B. Teplow, *Proc. Natl. Acad. Sci. USA* **1996**, *93*, 1125–1129.
[25] J. D. Harper, P. T. Lansbury, *Annu. Rev. Biochem.* **1997**, *66*, 385–407.
[26] D. M. Blow, N. E. Chayen, L. F. Lloyd, E. Saridakis, *Protein Sci.* **1994**, *3*, 1638–1643.
[27] K. A. Ramirez-Aguilar, K. L. Rowlen, *Langmuir* **1998**, *14*, 2562–2566.
[28] J. D. Harper, S. S. Wong, C. M. Lieber, P. T. Lansbury, *Biochemistry* **1999**, *38*, 8972–8980.
[29] S. Y. Fung, C. Keyes, J. Duhamel, P. Chen, *Biophys. J.* **2003**, *85*, 537–548.
[30] A. Aggeli, I. A. Nyrkova, M. Bell, R. Hardling, L. Carrick, T. C. B. McLeish, A. N. Semenov, N. Boden, *Proc. Natl. Acad. Sci. USA* **2001**, *98*, 11857–11862.
[31] H. K. Narang, *J. Neuropathol. Exp. Neurol.* **1980**, *39*, 621–631.
[32] P. A. Merz, H. M. Wisniewski, R. A. Somerville, S. A. Bobin, C. L. Masters, K. Iqbal, *Acta Neuropathol.* **1983**, *60*, 113–124.
[33] H. Puchtler, F. Sweat, M. Levine, *J. Histochem. Cytochem.* **1962**, *10*, 355–364.
[34] A. Wada, *Adv. Biophys.* **1976**, *9*, 1–63.
[35] M. Niwa, M. Morikawa, N. Higashi, *Langmuir* **1999**, *15*, 5088–5092.

Received: May 31, 2005
Published online: September 15, 2005

